

PROCEEDINGS OF SPIE

SPIEDigitalLibrary.org/conference-proceedings-of-spie

Characterization of varied geometry shape memory alloy beams

Lynn Gravatt, James Mabe, Frederick Calkins, Darren Hartl

Lynn M. Gravatt, James H. Mabe, Frederick T. Calkins, Darren J. Hartl,
"Characterization of varied geometry shape memory alloy beams," Proc. SPIE
7645, Industrial and Commercial Applications of Smart Structures
Technologies 2010, 76450U (29 March 2010); doi: 10.1117/12.847635

SPIE.

Event: SPIE Smart Structures and Materials + Nondestructive Evaluation and
Health Monitoring, 2010, San Diego, California, United States

Characterization of Varied Geometry Shape Memory Alloy Beams

Lynn M. Gravatt, James H. Mabe, and Frederick T. Calkins
The Boeing Company, Seattle, WA, U.S.A

Darren J. Hartl
Texas A&M University, College Station, TX, U.S.A

ABSTRACT

Shape Memory Alloys (SMA) have proven to be a lightweight, low cost alternative to conventional actuators for a number of commercial applications. Future applications will require a more complex shape changes and a detailed understanding of the performance of more complex SMA actuators is required. The purpose of this study is to validate engineering models and design practices for SMA beams of various configurations for future applications. Until now, SMA actuators have been fabricated into relatively simple beam shapes. Boeing is now fabricating beams with more complicated geometries in order to determine their strength and shape memory characteristics. These more complicated shapes will allow for lighter and more compact SMA actuators as well as provide more complex shape control. Some of the geometries evaluated include vertical and horizontal I-beams, sine wave and linear wave beams, a truss, and a beam perforated with circular holes along the length.

A total of six beams were tested; each was a complex shape made from 57% Nickel by weight with the remainder composed of Titanium (57NiTi). Each sample was put through a number of characterization tests. These include a 3-point bend tests to determine force/displacement properties, and thermal cycling under a range of isobaric loads to determine actuator properties. Experimental results were then compared to modeled results. Test results for one representative beam were used to calibrate a 3-D constitutive model implemented in an finite element framework. It is shown that the calibrated analysis tool is accurate in predicting the response of the other beams. Finally, the actuation work capabilities of the beams are compared using a second round of finite element analysis.

Keywords: Shape Memory Alloys, SMA, Smart Structures, Active Materials, Nitinol, NiTi, Actuators

1. INTRODUCTION

Since their discovery by Buehler in 1961, Shape Memory Alloys have shown great promise as actuators¹. For over 25 years, Boeing has been emerging as a pioneer in the development of SMA alloys for aerospace applications. In the early 1990's, large scale programs such as SAMPSON showed that fully integrated SMA wire bundles could provide a fighter aircraft with Variable Engine Inlet capabilities². Since that time, Boeing's expertise in the area of SMAs has continued to grow with programs like the Variable Area Chevron, where SMA flexures were used to morph part of the engine structure for noise reduction³. In addition, Boeing and it's collaborators are doing extensive work to improve the modeling of SMA structures^{5,7}. These capabilities have progressed to the point that the stress and strain distributions throughout complex geometries (geometries for which a straightforward analytical solutions of stress-strain response cannot be obtained) can be accurately predicted. This paper will show the force and displacement capabilities of SMA beams with complex geometries as well as how such outputs can be accurately modeled using FEA. Ultimately this serves as a tool for developing future SMAs for a wider range of applications.

Industrial and Commercial Applications of Smart Structures Technologies 2010,
edited by M. Brett McMickell, Kevin M. Farinholt, Proc. of SPIE Vol. 7645,
76450U · © 2010 SPIE · CCC code: 0277-786X/10/\$18 · doi: 10.1117/12.847635

Proc. of SPIE Vol. 7645 76450U-1

2. EXPERIMENTAL SET-UP

Three point bend tests were conducted on six SMA beams of complex geometries. The SMA beams are shown below in Figure 1. The shapes include: 1) a linear wave, 2) a horizontal I-beam, 3) a sine wave, 4) a rectangular beam with circular holes through the width, 5) a rectangular beam with triangular holes through the width (a truss), and 6) a vertical I-beam.

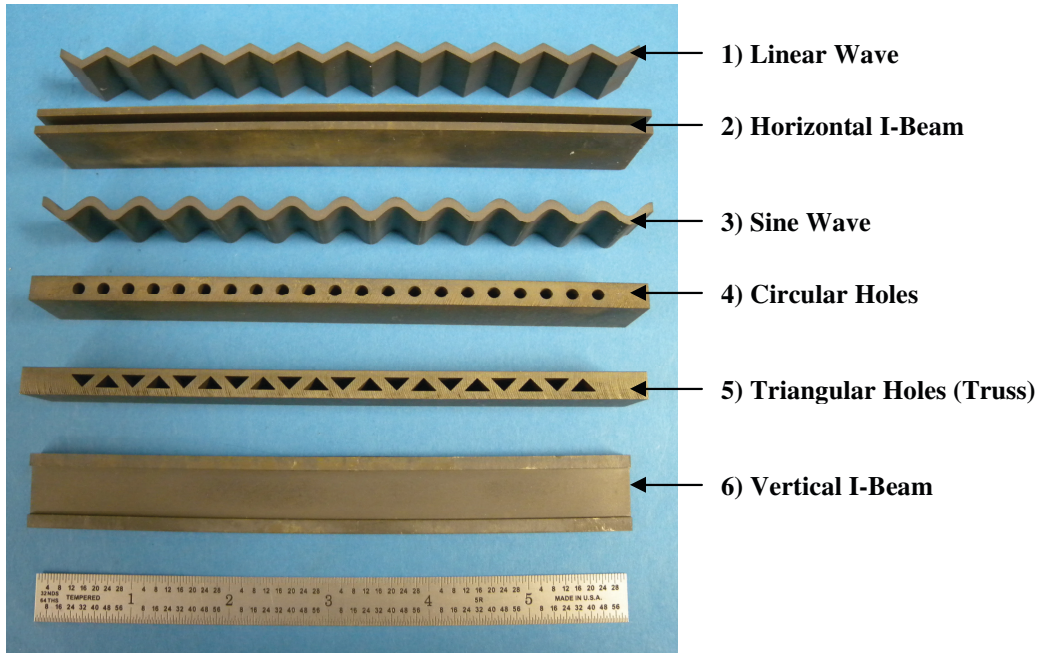


Figure 1. Complex SMA beam geometries considered.

Each sample was placed into a 3-point bend setup. Before testing, resistive heating strips were attached to each beam and three thermocouples were attached at various locations along the length of each beam. Figures 2a and 2b show the horizontal and vertical I-beams loaded into the test fixture.

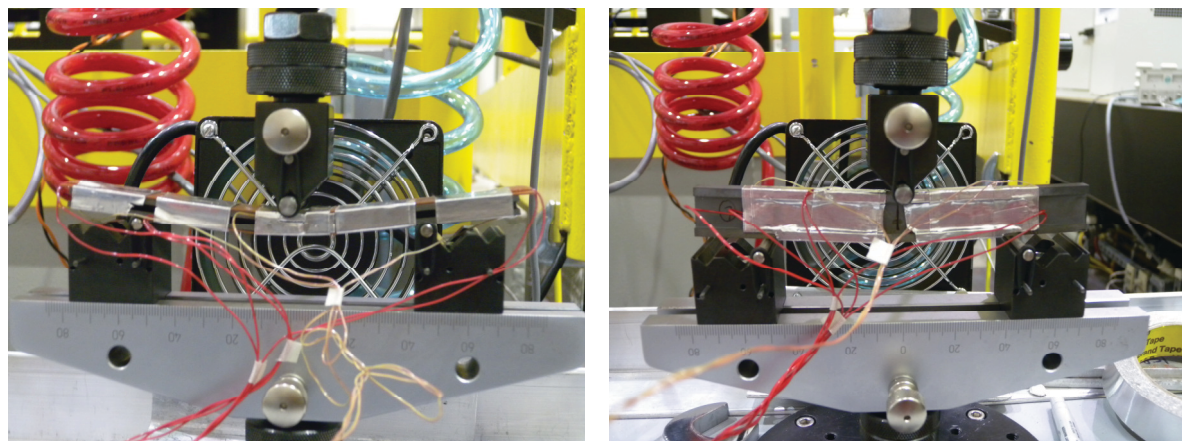


Figure 2. I-Beams loaded into 3-point bending apparatus.

Each beam then thermally cycles through phase transformation five times. During each cycle, a different constant load was applied. Loads corresponding to roughly 0, 35, 70, 140, and 210 MPa maximum stress were applied. To determine the testing loads in a consistent manner, each beam was approximated as having a rectangular cross-section with outer dimension as taken from the actual beam. The Euler-Bernoulli beam equations were used to determine the load corresponding to the stresses above. Because many of the shapes do not have an exact load-stress solution, the loads used only roughly correspond to the target stresses. However, the quick estimate ensured the loads were within the workable range of the beam. For the scope of this paper, only the data for the two highest loads will be considered as they represent loads the beams would likely see in aerospace applications.

3. EXPERIMENTAL RESULTS

Figures 3a and 3b show the thermomechanical response of the horizontal and vertical I-beams, respectively, where the two highest constant load applied to each are clearly noted. The results show vastly different force and displacement capabilities for the two beams of roughly the same exterior dimensions. The horizontal I-beam shows a much lower working load and higher displacement capabilities than the vertical I-beam. This side by side comparison of two similarly sized SMA beams shows the versatility of SMA when formed into various structural components. For applications where low force and high displacement are important, the horizontal I-beam would be a good choice; if high forces are required but large displacements are not, the vertical I-beam would be a better choice.

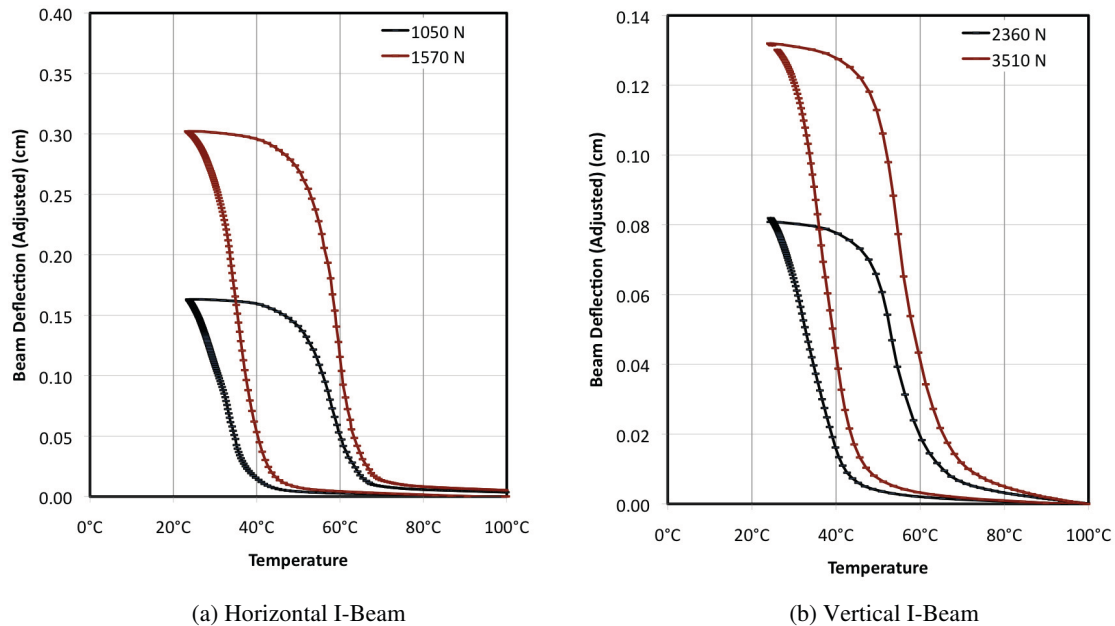


Figure 3. Experimental response of I-Beams. Note the difference in the deformations.

The next set of beams tested included the sine wave and the linear wave. The responses of the two beams are compared in Figures 4a and 4b.

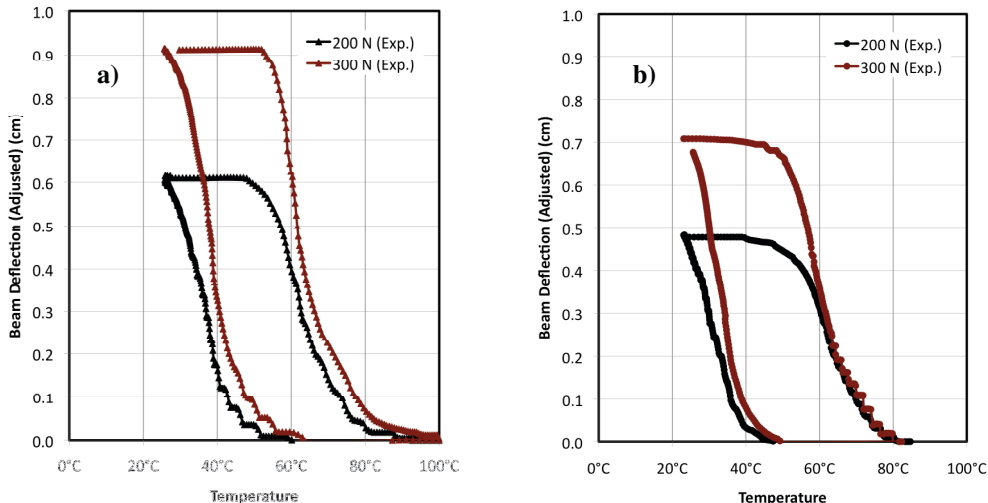


Figure 4. Experimental response of the a) linear wave and b) sine wave.

These two beams have the same outer dimensions so a direct comparison of their performance is appropriate. The data shows that given the same load, the linear wave produced more displacement. Modeling predictions, which will be discussed in subsequent sections of this paper, indicate that these two beams should be producing nearly the same amount of displacement. This deviation from expectations shows the variability in SMA-based active structural components. There are many potential explanations for why the sine wave “underperformed”, all of which require more investigation. Any small variation in the material due to processing, for example, might cause the performance of a given sample to suffer. As previously stated, further investigation is required.

The responses of beams with the round holes and triangular holes (the truss) are compared in Figure 5. The results show that for the same loads, the beam with the round holes appears to have produced more displacement than the beam with triangular holes. In this case, we believe this a thermal effect. The conditions in the lab the day the triangular beam was tested were warmer, and thus the sample couldn't be cooled as much as would have been desired. It is believed that with more cooling, the displacements of the “truss” beam would have reached the same levels as those exhibited by the hole perforated beam.

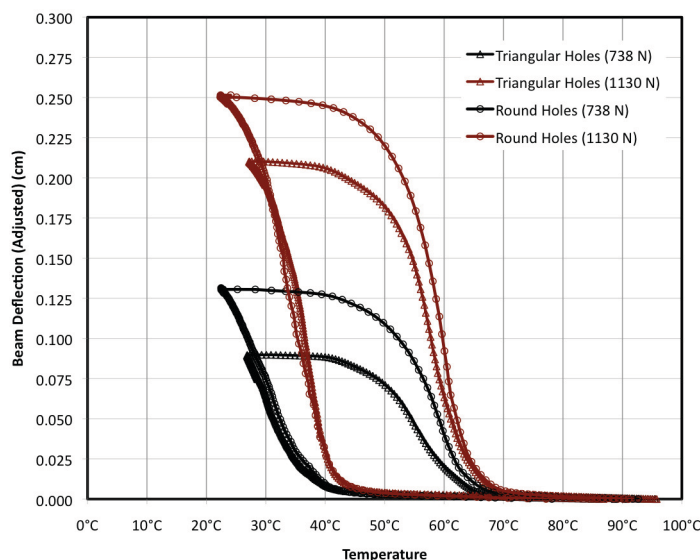


Figure 5. Experimental response from round holes and triangular holes.

Collectively, these results demonstrate the versatility of these SMA beam geometries. The wave beams, for example, exhibited the biggest deformations. In the case of the two I-beams, the results show how versatile SMA beams can be depending on the geometries. It shows that for virtually any application where actuation is needed, an appropriate beam can be selected or designed. Force and displacement requirements, as well as physical space limitations within the application, should determine what geometry will be chosen for a given actuator. The next portion of the paper will discuss the FEA modeling of these beams.

4. NUMERICAL ANALYSIS

Having completed the experimental study of the various active SMA beams, we now shift focus to the numerical analysis of these same beam configurations. A validated and robust method of numerical analysis is considered a key goal in the continued development of active structures technologies. Ideally, such a tool should allow the actuation response prediction of a wide range of 3-D SMA configurations. With regard to the topic at hand, the ability to accurately predict active beam responses will allow designers and engineers to choose the best beam configurations for a given bending application without the need for experimentally testing every possible option. As different applications impose different engineering constraints, an analysis tool can help streamline the process of optimizing beam shapes in terms of some measure (e.g., predicted actuator work output per unit weight).

To this end, a 3-D constitutive model for SMAs (as implemented in an FEA framework) was used to model the response of each of the preceding six beams. Specifically, a model based on the early work of Boyd and Lagoudas⁴, and further improved elsewhere in the literature⁵, is chosen. This model and its implementation into an Abaqus Unified FEA framework⁶ have already proven to be accurate in the modeling of complex SMA actuators, especially those utilizing bending⁵. To begin, the response of a single beam configuration (Horizontal I-Beam) is considered, and the input parameters of the model are tuned until this response is accurately captured. This process corresponds to *model calibration*. Following this, the parameters are *held constant*, and the other five beams are modeled using these parameters, where the predictions of the analysis are compared to the experimental responses described above. This corresponds to *predictive model validation*. Finally, the validated model is used to predict the response of the six beams under a consistent set of loading conditions not yet experimentally considered, and it is shown that this allows direct comparison of the actuation responses of multiple beam configurations subject to comparable loads.

5. CALIBRATION AND VALIDATION

When calibrating the implemented constitutive model for analysis of 3-D configurations, it is generally most convenient to utilize test data from a set of 1-D (e.g., uniaxial) experiments. This approach has been successfully applied to the accurate calibration of the current model in previous studies^{2,7}. For the current work, however, such data was not available; no uniaxial tests have been performed on this 57NiTi SMA composition processed in the manner used to form these beams. Thus, an alternative method of calibration was required.

To determine the model parameters for the analysis of these six 57NiTi beams, the thermally-induced actuation response of a single representative beam was considered. By carefully tuning the assumed material properties, a set of model parameters was determined that resulted in a sufficiently close fit of analytical prediction to experimental data. For the current study, the Horizontal I-Beam was chosen as that representative beam. This is because: *i*) the loads applied to this beam are comparable to those applied to the Round Hole and Truss (Triangular Hole) beams, and *ii*) its cross-section is similar to that of the Vertical I-Beam. The resulting simulation results for the response of this beam are shown in Figure 6. Note that a close agreement between experiment and theory was obtained, and that the model is capable of capturing

both the smoothness of the response as well as the change in actuation deflection with varying loads⁵. Few if any other models in the literature are capable of capturing both.

Before continuing, it is important to describe the FEA model used to analyze this and the remaining five beams. Each beam model is constructed with the same dimensions as its experimental counterpart, and is discretized using 3-D quadratic reduced-integration elements (Abaqus designation C3D20R⁶). Large deformation theory (NLGEOM=YES) is utilized. The two upright supports are modeled by constraining the two lines of nodes nearest the two supports in the vertical direction. The distance between these supports varies from beam to beam and will be provided. The applied load is modeled by distributing the total load among all nodes spanning the width of the beam at its center (top surface). The magnitudes of the total loads were taken directly from the experimental loads previously discussed, and the temperature limits during cooling were taken from there as well. Finally, where noted, symmetry was exploited. In the specific case of the Horizontal I-Beam:

- 4088 elements were used, the uprights were taken to be 9.7 cm apart, and the entire beam was modeled (no symmetry was exploited).

The final set of material properties chosen (and used to provide the close match of Figure 6) are provided in Table 1. For a detailed description of these properties, the reader is referred to the literature⁵. In brief, they include the thermoelastic properties of each phase (Young's modulus, Poisson's ratio, and thermal expansion coefficient), the properties of the SMA phase diagram (transformation temperatures and slopes of the transformation surfaces), parameters describing the smoothness of the four corners of the hysteresis, and a function describing the dependence of the magnitude of transformation strain generation on the applied stress level. Note that these values provide a good prediction of structural and actuation responses but may not correspond to carefully measured experimental constitutive properties.

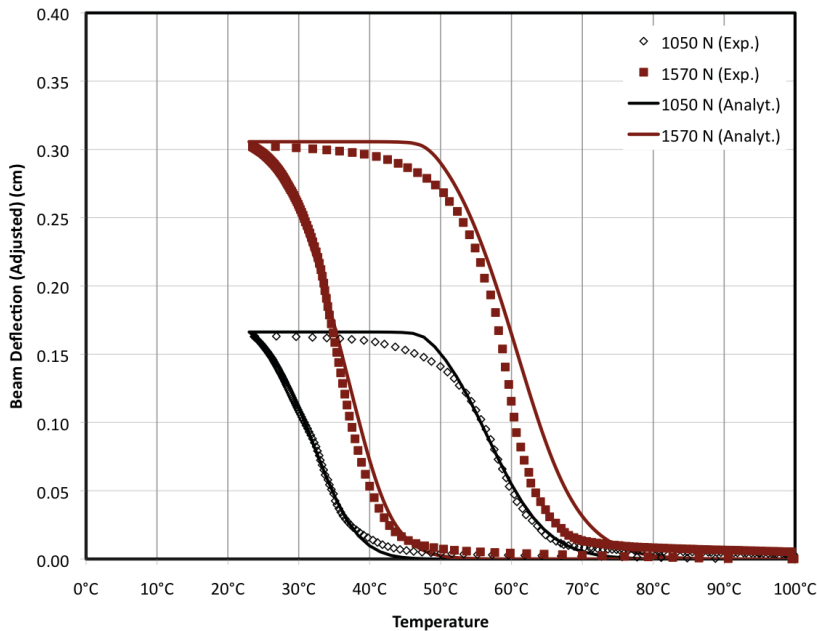


Figure 6 – Comparison of experimental and analytical responses of the Horizontal I-Beam (for fitting of model parameters).

Table 1 - Material properties determined by matching the experimental and analytical responses of the Horizontal I-Beam (see Reference 5 for a description of the parameters).

Property Name	Value	Units
$E^A = E^M$	48	GPa
$v^A = v^M$	0.33	
$\alpha^A = \alpha^M$	0.00	1/°C
M_s, M_f, A_s, A_f	35, 13, 30, 73	°C
$C^A = C^M$	13.8	MPa/°C
Calibration Stress	300	MPa
n_1, n_2, n_3, n_4	0.6, 0.2, 0.2, 0.2	
$H^{cur}(\sigma)$	$0, \sigma < 69$ $0.0095 \{1 - \exp[-0.03(\sigma - 69)]\}, \sigma \geq 69$	(σ in MPa)

Following the successful calibration of the model, the parameters of Table 1 were then *held fixed* and used in simulating of the response of the remaining five beam configurations. This provided a means of independent model (and parameter) validation, where a close match between experimental results and theoretical predictions indicated that the calibrated analysis tool could be trusted to provide meaningful predictive results. The reference mesh for each of the six beams is shown in Figure 7. Also shown is the distribution of *effective transformation strain* at the end of the cooling step under the application of the highest load considered for each beam (e.g., 1570 N for the Horizontal I-Beam). The effective transformation strain is a scalar measure of the magnitude of transformation strain defined in the Mises sense as:

$$\bar{\epsilon}' = \sqrt{\frac{2}{3} \boldsymbol{\epsilon}' : \boldsymbol{\epsilon}'},$$

where $\boldsymbol{\epsilon}'$ is the transformation strain tensor. Finally, note the location of the two supports at the bottom of each beam in Figure 7.

In general, each FEA model is constructed in the same manner as that used for the Horizontal I-Beam previously described. The unique model attributes applied to each beam are as follows:

- Vertical I-Beam: 3402 elements, 9.7 cm support spacing, no symmetries exploited;
- Round Holes: 22188 elements, 9.7 cm support spacing, symmetry about the beam half-width exploited;
- Triangular Holes: 5616 elements, 9.7 cm support spacing, symmetry about the beam half-width exploited;
- Linear Wave: 8640 elements, 8.9 cm support spacing, no symmetries exploited;
- Sinusoidal Wave: 6720 elements, 8.9 cm support spacing, no symmetries exploited;

The prediction results for each of the five beams are shown in Figure 8 – Figure 10. Figure 8 indicates that the calibrated model is quite accurate in the prediction in the response of the Vertical I-Beam. Likewise, Figure 9a and Figure 9b indicate that the responses of the Round Hole and Triangular Hole (respectively) are also accurately captured. The results from the analysis of the two “wave” beams are shown in Figure 10. While a close match is observed for the Linear Wave, experimental issues with the measurement of temperature or possible variations in the material processing are thought to be the cause of for the less impressive prediction of the Sinusoidal Wave response. It is interesting to note that in none of the six analysis cases does the beam complete forward transformation into martensite during cooling. The ability to capture the actuation deflection is dependent on the accurate modeling of partial transformation.

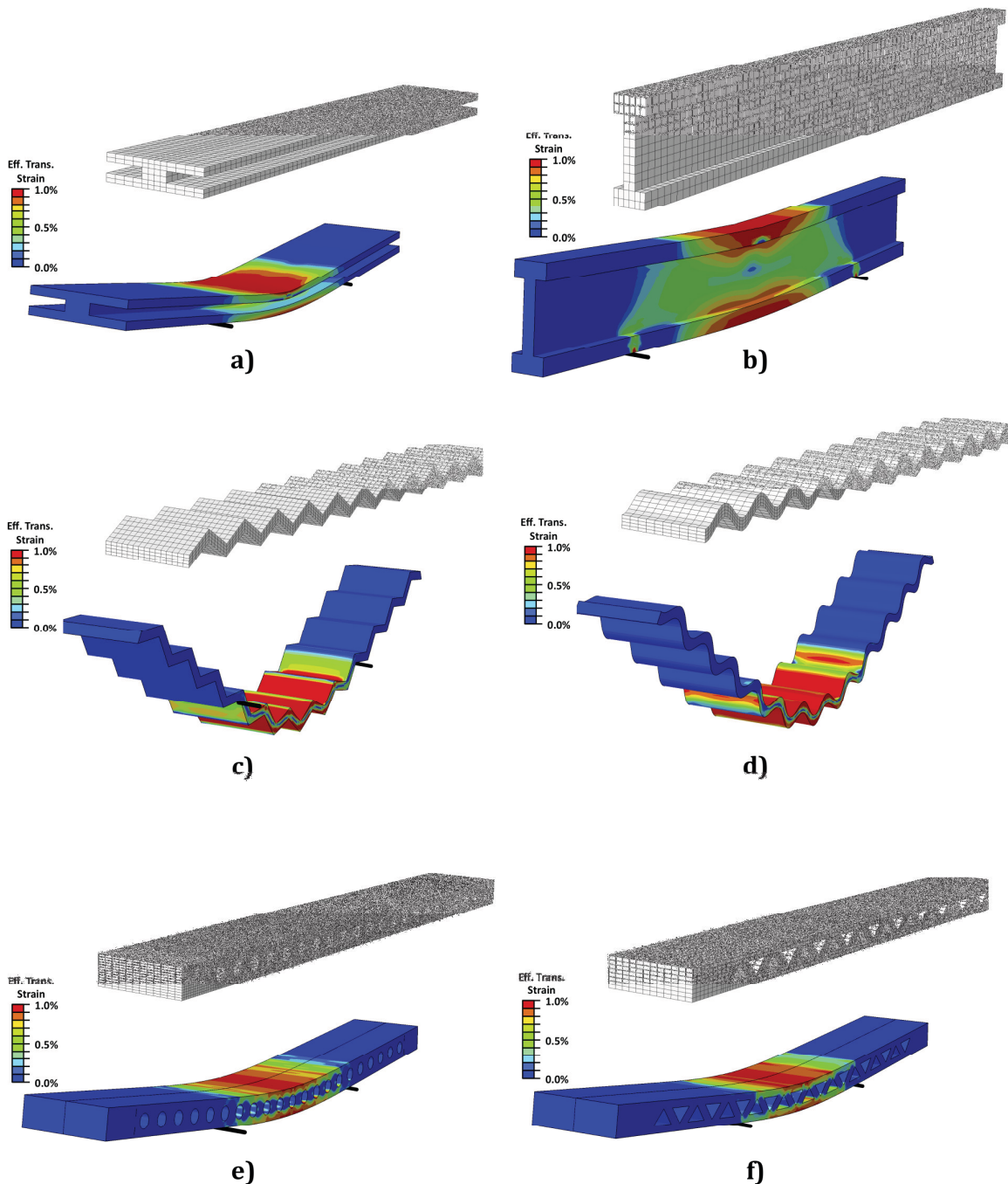


Figure 7 - Reference mesh and effective transformation strain contours from the FEA analysis of the six SMA beams. Specifically, they are: a) Horizontal I-Beam, b) Vertical I-Beam, c) Linear Wave, d) Sinusoidal Wave, e) Round Holes, and f) Triangular Holes. Effective transformation strain contours are captured at end of cooling, highest applied constant load.

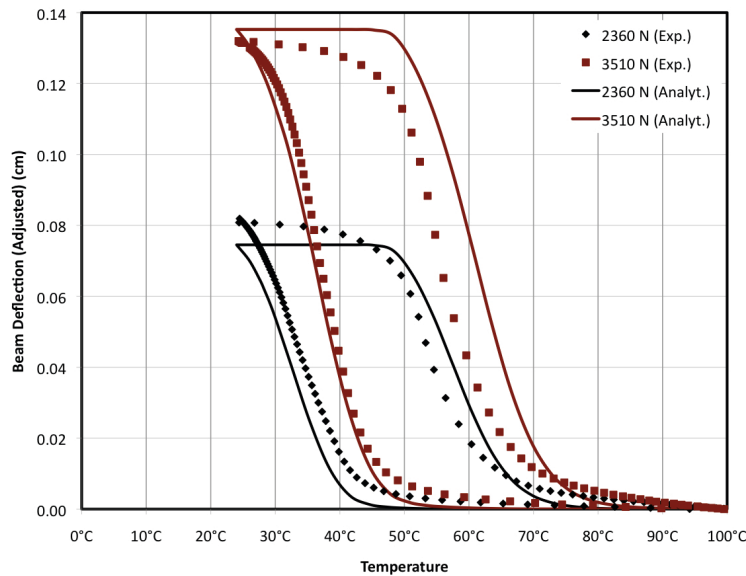


Figure 8 - Analytical prediction of the experimental actuation response of the Vertical I-Beam.

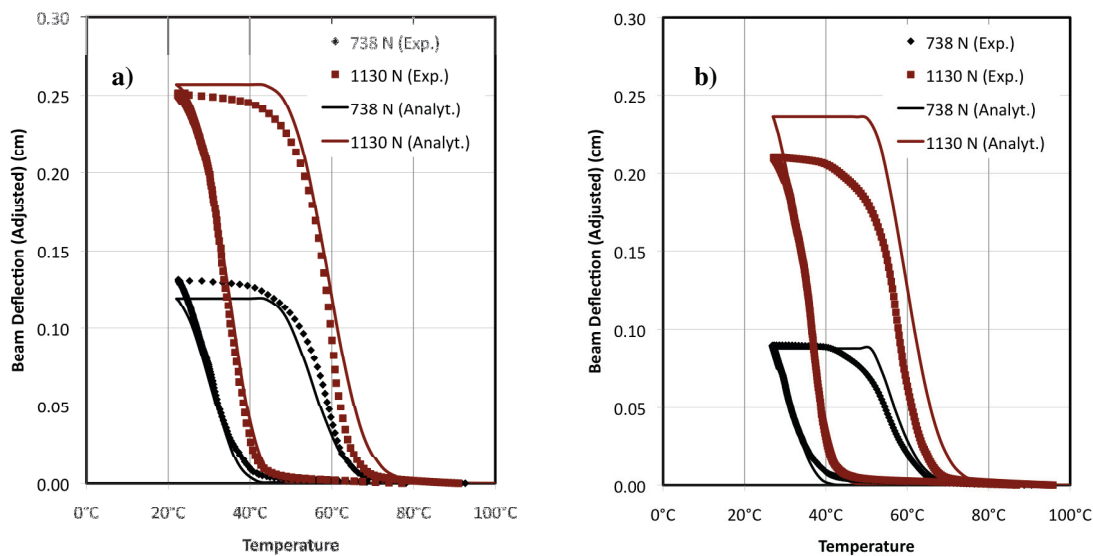


Figure 9 - Analytical prediction of the experimental actuation response of the
a) Round Hole and b) Triangular Hole Beams.

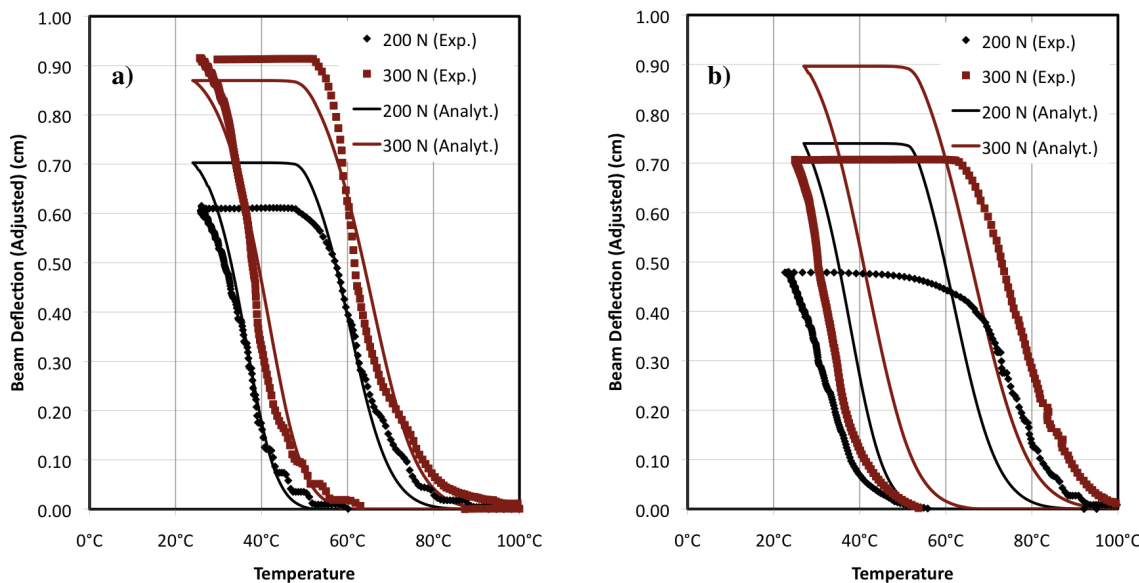


Figure 10 - Analytical prediction of the experimental actuation response of the "wave" beams
a) Linear Wave b) Sinusoidal Wave

6. PREDICTION OF ACTUATION RESPONSE

With the accuracy of the implemented model and chosen parameters satisfactorily validated, we conclude the current study of various active SMA beams configurations by demonstrating how the analysis tool might assist in the design of engineering applications by using it to directly compare the relative performance of the beams. As a measure for comparison, we choose to examine the work provided by the six beams during reverse transformation into austenite (i.e., during thermal actuation). Of course, the work output in any given beam varies greatly with applied load level; greater loads require more actuation force and also induce larger actuation deflections (as seen in the various figures above). To allow for a meaningful comparison across such varied beams, it was decided that the analysis of each would consider a constant force sufficient to induce a maximum stress of 30 ksi (207 MPa) somewhere in the beam (e.g., middle of the beam length, lower surface, extreme fiber for the I-beams). This "load at 30 ksi maximum stress" was found by performing FEA on each of the beams under elastic loading, and the maximum stress was taken to be the highest Mises equivalent stress computed at any integration point in the FEA model.

As a summary, the loads required to induce 30 ksi (Mises equivalent) stress in each of the six beams are given in Table 2. Also provided is the *active volume* of each beam, which considers only the volume of the beam in the region spanning from one vertical support to the other. A seventh beam having the same length and a simple rectangular cross-section (1.22 cm by 0.66 cm) is also considered. Note that experimental investigation of these loads has not been performed to date for any of the seven beams; the following results represent purely theoretical predictions.

Table 2 - Input parameters and results for the actuator work and specific actuator work density analyses of seven SMA beams.

Beam Configuration	Load @ 30 ksi Max [N]	Active Volume [cm ³]	Full Trans. Actuation Work [J]	Spec. Actuation Work Density [J/kg]
Horiz. I-Beam	1219	10.9	2.77	39.1
Vert. I-Beam	2793	6.70	2.93	67.2
Round Hole	1045	9.34	2.58	42.4
Triangular Hole	1031	8.65	2.43	43.1
Linear Wave	173	3.07	1.09	54.5
Sinusoidal Wave	129	3.07	0.63	31.3
Rectangle	676	7.21	1.92	41.1

The work output capability of the beams was then assessed by analyzing the thermally-induced actuation deflection provided by each beam under an applied constant load as determined from Table 2. The *full transformation actuation work* is then taken to be the product of the constant applied load with the deflection provided by the beam during thermally-induced reverse transformation from full martensite into full austenite (i.e., during heating). This value is provided for each beam in Table 2. As a method of visual comparison, the evolution of this work output with temperature (during the process of transformation) is plotted for each beam in Figure . The saturated level of work output corresponds to the value reported in Table 2.

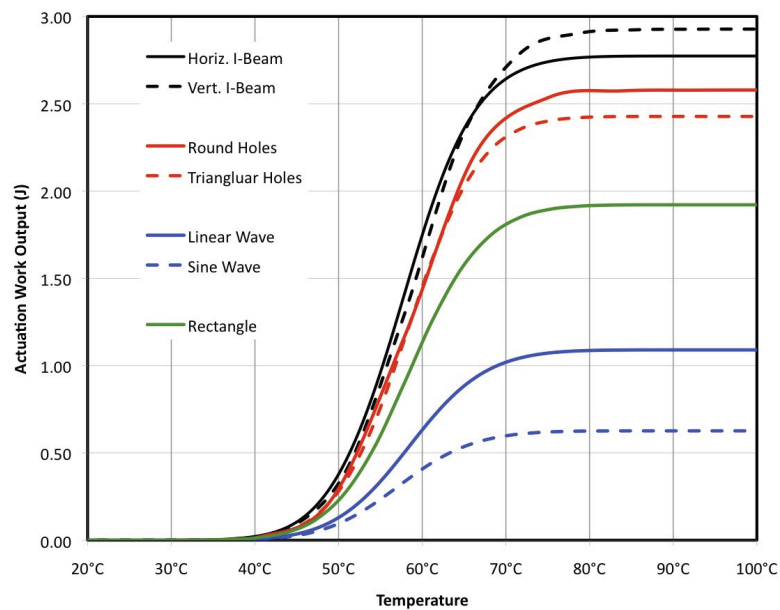


Figure 11 - Evolution of work output for each beam as a function of temperature (for an actuation load inducing 30 ksi (207 MPa) maximum stress).

In the aerospace industry, the issue of actuator weight is often one important design consideration among others. With this in mind, we scale the work provided by each beam by its active weight (computed by multiplying its active volume with a nominal density⁸ of 6500 kg/m³). This is referred to as the *specific actuation work density*, and its value for each beam is also given in Table 2. As a point of comparison, it is interesting to note that a similar SMA composition (Ni60Ti) has been shown to provide a specific actuation work density of ~200 J/kg under pure uniaxial loading at 200 MPa (calculated by taking the product of constant actuation stress with actuation strain and dividing by material density). However, although the beams consistently provide less work density than their constituent material under homogenous loading, they do provide a large increase in deformation motion and can provide 3-D force distributions.

Examining the last two columns of Table 2, we see little correlation between actuator work output and specific actuator work density. It is difficult to produce meaningful trends from these predictions, making the full 3-D analysis tool important to the design process. For example, the Vertical I-Beam, while providing the least deflection, provides the most work and highest specific work density (due to its large force capability). The Linear Wave, however, produces ~1/3 the work output, but ranks second in specific work density (due to its lightweight configuration). The plain rectangular cross-section, being fully dense, provides only a moderate level of work and a moderate specific work density. Given these results, it is clear that any productive effort to optimize beam geometry for a given application would benefit greatly from the output of this validated 3-D analysis tool.

7. CONCLUSIONS

Currently, advancements in the aerospace technology have made once futuristic ideas such as morphing aerostucture a reality. As this technology progresses, lightweight and powerful actuators will be needed. SMA will play an important role in this effort. We have shown that Boeing will be able to meet the demands of the industry by providing complex powerful actuators to fit almost any application. In addition, by partnering with TA&M and other universities, the capability to predict an actuators performance with accuracy has been developed. These modeling practices will save the industry time and money as it eliminates the need for trial and error when determining actuator performance.

8. REFERENCES

- 1 G. Kauffman, I. Mayo, "The Story of Nitinol: the serendipitous discovery of the memory metal and it's applications," *The Chemical Educator*, Vol 2, No 2, June 1997.
- 2 D. Pitt, J. Dune, E. White, and E. Garcia, "SAMPSON smart inlet SMA powered adaptive lip design and static test," *Proceedings from the 42nd AIAA Structures, Dynamic Structures, and Materials Conference, Seattle, WA, 16-12 April 2001*, pp. 1-11, 2001.
- 3 J. Mabe, F.T. Calkins, R. Ruggeru, "Fulle-scale Flight Tests of Aircraft Morphing Structures using SMA actuators," *SPIE, Smart Structures and Materials/NDE, San Diego. CA, 18-22 March 2007*, paper 6525-48.
- 4 J. G. Boyd, D. C. Lagoudas, "A thermodynamical constitutive model for shape memory materials. Part I. The monolithic shape memory alloy," *International Journal of Plasticity* **12** (6), pp. 805–842, 1996.
- 5 D. Hartl, D. Lagoudas, J. Mabe, F. Calkins, J. Mooney, "Use of Ni60Ti shape memory alloy for active jet engine chevron application, Part II: Experimentally validated numerical analysis," *Smart Materials and Structures* **19** (1), 2010.
- 6 Abaqus, Analysis User's Manual, Dassault Systèmes of America Corp., Wood- lands Hills, CA, 2009.
- 7 D. Hartl, D. Lagoudas, J. Mabe, F. Calkins, "Use of Ni60Ti shape memory alloy for active jet engine chevron application, Part I: Thermomechanical characterization," *Smart Materials and Structures* **19** (1), 2010.
- 8 D. Lagoudas (Ed.), *Shape Memory Alloys: Modeling and Engineering Applications*, Springer-Verlag, New York, 2008.